

Torque Generation in F₁-ATPase Devoid of the Entire Amino-Terminal Helix of the Rotor That Fills Half of the Stator Orifice

Ayako Kohori,^{†Δ} Ryohei Chiwata,^{†Δ} Mohammad Delawar Hossain,^{†‡} Shou Furuike,[†] Katsuyuki Shiroguchi,[†] Kengo Adachi,[†] Masasuke Yoshida,^{§¶} and Kazuhiko Kinoshita, Jr.^{†*}

[†]Department of Physics, Faculty of Science and Engineering, Waseda University, Shinjuku-ku, Tokyo, Japan; [‡]Department of Physics, School of Physical Sciences, Shahjalal University of Science and Technology, Sylhet, Bangladesh; [§]ATP Synthesis Regulation Project, ICORP, Japan Science and Technology Agency (JST), Aomi, Koto-ku, Tokyo, Japan; and [¶]Department of Molecular Bioscience, Kyoto Sangyo University, Kamigamo, Kyoto, Japan

ABSTRACT F₁-ATPase is an ATP-driven rotary molecular motor in which the central γ -subunit rotates inside a cylinder made of $\alpha_3\beta_3$ subunits. The amino and carboxyl termini of the γ rotor form a coiled coil of α -helices that penetrates the stator cylinder to serve as an axle. Crystal structures indicate that the axle is supported by the stator at two positions, at the orifice and by the hydrophobic sleeve surrounding the axle tip. The sleeve contacts are almost exclusively to the longer carboxyl-terminal helix, whereas nearly half the orifice contacts are to the amino-terminal helix. Here, we truncated the amino-terminal helix stepwise up to 50 residues, removing one half of the axle all the way up and far beyond the orifice. The half-sliced axle still rotated with an unloaded speed a quarter of the wild-type speed, with torque nearly half the wild-type torque. The truncations were made in a construct where the rotor tip was connected to a β -subunit via a short peptide linker. Linking alone did not change the rotational characteristics significantly. These and previous results show that nearly half the normal torque is generated if rotor-stator interactions either at the orifice or at the sleeve are preserved, suggesting that the make of the motor is quite robust.

INTRODUCTION

F₁-ATPase (F₁) is a rotary molecular motor driven by ATP hydrolysis, with the minimal subunit composition of $\alpha_3\beta_3\gamma$ (1–7). In the crystal structures of mitochondrial F₁ (MF₁) (Fig. 1), the γ rotor deeply penetrates the central hole of the hexameric stator cylinder made of three α and three β subunits arranged alternately (8,9). Each time ATP is hydrolyzed in one of the three catalytic sites that are hosted primarily by a β -subunit (8), the rotor rotates 120° counterclockwise when viewed from above in Fig. 1 (10). The amino- (N-) and carboxyl- (C-) termini of γ form an antiparallel coiled coil of long α -helices (Fig. 1, *yellow* and *orange*, respectively) that penetrates the stator cylinder to serve as an axle. The stator supports the axle at the upper orifice and at the bottom, the bottom contacts being mainly to the longer C-terminal helix. Because the bottom support consists of the “hydrophobic sleeve” and the “catch loop”

described in the original crystal structure (8), we call the upper and lower contact regions the “orifice” and “sleeve” in this article (Fig. 1, *blue* and *dark green atoms*; these atoms are within 0.5 nm of a rotor atom and delineate the two contact regions).

Previously we truncated most of the axle step by step, starting with the C-terminus and then keeping the tips of the N- and C-terminal helices at the same level (11,12). The truncations were made in F₁ derived from a thermophilic *Bacillus* PS3 (TF₁), which is homologous with MF₁ in sequence and structure (13). The last product that still rotated was $\gamma\Delta N22C43$, where 22 N-terminal and 43 C-terminal residues of γ were deleted genetically (Fig. 1 B). This “axle-less” construct rotated in the correct direction for >100 revolutions, although the speed was much lower than the wild-type and was ~1 revolution/s. The surprise was that the remaining rotor head, which must have lost all the sleeve interactions with the stator and nearly half of the orifice interactions, was not detached during the rotation. In the MF₁ structure shown, 233 γ atoms are within 0.5 nm of a stator atom, excluding hydrogen, and 76 and 111 of these are on the N- and C-terminal helices, respectively. The axle-less construct lacked 159 of the contacting atoms (*gray* in Fig. 1 B) and, of the remaining 74, 28 (38%) are on the N-terminal helix (Fig. 1 B, *left dotted ellipse, dark yellow atoms*). This construct could rotate only a 40-nm gold bead, for which viscous drag is almost negligible. Rotation of larger beads requires a significant torque, and we observed rotation of a duplex of 0.29- μ m beads only up to $\gamma\Delta N11C32$. The torque $\gamma\Delta N11C32$ generated was ~20 pN·nm, i.e., half of the wild-type torque, and 62 (49%) of the remaining 126

Submitted March 17, 2011, and accepted for publication May 3, 2011.

^Δ Ayako Kohori and Ryohei Chiwata contributed equally to this work.

*Correspondence: kazuhiko@waseda.jp

Shou Furuike's present address is Faculty of Physics, Osaka Medical College, Takatsuki City, Osaka, Japan.

Katsuyuki Shiroguchi's present address is Department of Chemistry and Chemical Biology, Harvard University, Cambridge, MA.

Kengo Adachi's present address is Department of Physics, Gakushuin University, Mejiro, Toshima-ku, Tokyo, Japan.

This is an Open Access article distributed under the terms of the Creative Commons-Attribution Noncommercial License (<http://creativecommons.org/licenses/by-nc/2.0/>), which permits unrestricted noncommercial use, distribution, and reproduction in any medium, provided the original work is properly cited.

Editor: David D. Hackney.

© 2011 by the Biophysical Society
0006-3495/11/07/0188/8 \$2.00

doi: 10.1016/j.bpj.2011.05.008

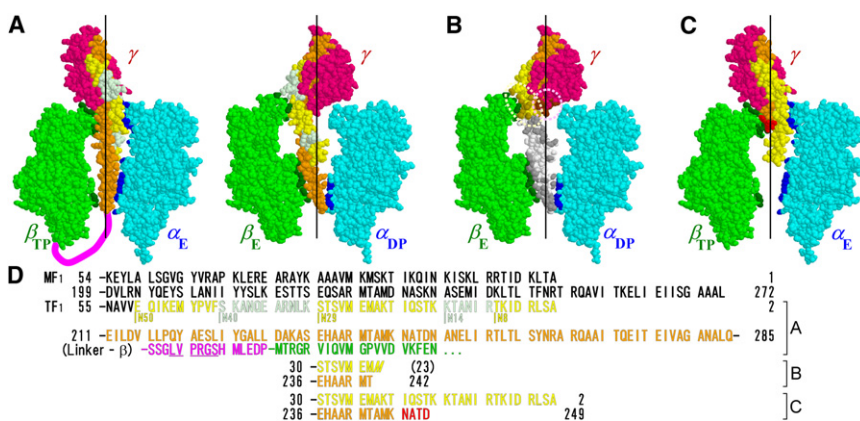


FIGURE 1 Design of truncation mutants based on a crystal structure of MF₁ (9). (A) Truncations of γ N-terminus (this study). The central γ subunit (dark pink) and an opposing pair of a β subunit (green) and an α subunit (cyan) are shown. The α and β subunits are designated according to the nucleotide bound in the original structure (8): TP, ATP (analog); DP, ADP; and E, empty. The C-terminal α -helix of γ is orange, and the N-terminal helix is yellow with intervening light gray indicating the positions of truncation as diagrammed in D. The magenta line represents the 15-residue peptide linker. Dark green and blue atoms are those within 0.5 nm of an atom in γ (excluding hydrogen). The black vertical line shows a putative rotation axis (35). (B) An axle-less construct in which 22 N-terminal and 43

C-terminal residues of γ were deleted, as shown in D; the terminal Met at position 23 was found unprocessed (12). Dark green and blue atoms are those within 0.5 nm of an atom in γ (excluding hydrogen). The black vertical line shows a putative rotation axis (35). (C) A construct in which 36 C-terminal residues of γ were deleted (14); terminal sequence in D. Further truncation of the four red residues resulted in a subcomplex that could not rotate a 0.29- μ m bead duplex. (D) N- and C-terminal sequences of the γ subunits of MF₁ and TF₁, showing the positions of truncation and the linker (thrombin site underlined) sequence for A. The sequence for TF₁ starts from 2, because we count from the first Met, which is processed in the wild-type but not in some mutants (12). See Table S1 for the entire sequence.

contacts are on the N-terminus. The construct $\gamma\Delta$ N0C36 (Fig. 1 C) could also generate approximately half the wild-type torque (14), suggesting that the middle portion of either the N- or C-terminal helices does not contribute to torque generation, whereas the sleeve interactions at the C-terminal tip are essential for full torque production (11). Thus, we expected that the contacts between the stator and the N-terminal helix that fills half of the orifice would be important for torque generation in F₁. Indeed, in the orifice region, the C-terminal helix does not make extensive contacts with the stator, at least in the crystal structures. Most of the contacts other than the N-terminal helix are on the conical entrance of the orifice (Fig. 1 B, right dotted ellipse, brown atoms).

The importance of the γ N-terminus in catalysis and rotation has been a focus in many studies. Deletion of seven γ N-terminal residues in *Escherichia coli* F₁ (EF₁) failed to assemble F₁ complex on membranes (15). *E. coli* ATP synthase in which γ Met-23 in the orifice was replaced with Arg or Lys exhibited inefficient energy coupling between ATP hydrolysis and H⁺ translocation (16), although in isolated EF₁ the Met-23Lys mutation did not affect torque production (17). The γ Met-23Lys mutation in *Rhodobacter capsulatus* ATP synthase significantly impaired the activation of ATPase activity by proton motive force (18). In EF₁, substitution of γ Lys-9 with Ile to remove the salt bridge with β Asp-372 decreased ATPase activity twofold, and substitution of γ Ser-12 with Ala to remove the hydrogen bond with β Asp-372 resulted in the decrease of succinate-dependent growth of *E. coli* by two orders of magnitude (19). Deletion of 20 N-terminal residues of chloroplast F₁ retained only ~6% of ATPase activity (20). Mitochondrial ATP synthase in yeast could be assembled upon deletion of nine N-terminal residues but failed when 20 residues were deleted (21).

Here, we investigated the role of the N-terminal α -helix of the γ -subunit by truncating it stepwise, starting with the axle

portion, continuing through the orifice region, and ending in the removal of all 50 of the residues comprising the N-terminal helix and containing the 76 contacting atoms (Fig. 1 A). All N-terminal truncation mutants were active, with reduced functionality. In hopes of reducing the problem of subcomplex instability encountered in previous truncation mutants, we genetically connected the γ C-terminus to the β N-terminus with a peptide linker (Fig. 1, A and D, magenta). We anticipated that linking would not abolish rotation, because disulfide bridging between the γ N-terminal tip and a residue in β does not impair catalysis and rotation (22). Indeed, the peptide linkage had minimal effect. The 50-deletion mutant (β - $\gamma\Delta$ N50) rotated with an unloaded speed a quarter of the wild-type speed and generated approximately half the wild-type torque. The major loss of orifice interactions is tolerable, at least as long as the C-terminal tip is preserved. The rotary mechanism of the F₁ motor seems quite robust, allowing deletions of many apparently crucial interactions.

MATERIALS AND METHODS

Molecular genetics

Mutations were made on plasmid pKABG1/HC95 (23,24), which carries genes for the α - (C193S), β - (His₁₀ at N-terminus), and γ (S107C, I210C)-subunits of TF₁, which we regard as the wild-type. On the plasmid, the three genes are arranged in the order α , γ , and β . First, we introduced His₆-tag at the N-terminus of the α -subunit. Then we connected the C-terminus of γ and the N-terminus of β (ignoring the His₁₀-tag) with the peptide linker (Fig. 1 D, magenta). From this construct, the γ N-terminus was truncated essentially as described (12). Mutations were confirmed by DNA sequencing (see the deduced amino-acid sequence in Table S1 in the Supporting Material).

Purification and biotinylation of mutant TF₁

Wild-type and mutant TF₁ were expressed in *E. coli* strain JM103, purified and biotinylated basically as described (14,25) but without heat treatment

and without butyl column treatment, which would remove bound nucleotide almost completely. Briefly, the *E. coli* cell lysate was purified on a Ni²⁺-nitrilotriacetic acid (Ni²⁺-NTA) column (Qiagen, Hilden, Germany) and stored as ammonium sulfate precipitate at 4°C. Before use, the sample was passed through a size-exclusion column (Superdex 200 HR 10/300, GE Healthcare, Uppsala, Sweden) equilibrated with buffer A (100 mM potassium phosphate, pH 7.0, and 2 mM EDTA) to obtain pure $\alpha_3\beta_3\gamma$ complex.

For observation of rotation, purified F₁ was biotinylated at the two cysteines (γ -107C and γ -210C) by incubation with a fourfold molar excess of 6-[N'-[2-(N-maleimide)ethyl]-N-piperazinylamide]hexyl-D-biotinamide (biotin-PEAC₅-maleimide, Dojindo, Kumamoto, Japan) in 2 mM MgCl₂, 100 mM potassium phosphate, pH 7.0, 50 mM KCl, and 10 mM Mops-KOH for 30 min at room temperature. Unreacted biotin was removed on the size-exclusion column equilibrated with buffer A.

Cleavage of the β - γ link, when attempted, was done immediately after biotinylation, before the final column purification. Thrombin from bovine plasma (Sigma Aldrich, St. Louis, MO) was added to 1–5 μ M F₁ in buffer A at 4 NIH units/nmol F₁ complex. After 10 min, the sample was applied to the size-exclusion column for purification. Longer treatment with thrombin, up to 18 h, did not change the cleavage pattern significantly (data not shown).

Measurement of hydrolysis activity

The rate of ATP hydrolysis at 2 mM MgATP was measured at 23°C by coupling the hydrolysis reaction with NADH consumption, as described (14). F₁ was added at a final concentration of 5–10 nM into an assay mixture consisting of 2 mM MgATP, 0.2 mM NADH, 1 mM phosphoenolpyruvate, 250 μ g mL⁻¹ pyruvate kinase (rabbit muscle, Roche Diagnostics, Mannheim, Germany), and 50 μ g mL⁻¹ lactate dehydrogenase (hog muscle, Roche Diagnostics), and 0.3% (w/v) lauryl dimethylamine oxide (LDAO, Calbiochem, La Jolla, CA) in buffer B (10 mM Mops-KOH, pH 7.0, 50 mM KCl, and 2 mM MgCl₂). The rate of hydrolysis was estimated over 5–15 s after mixing. F₁ treated with thrombin was biotinylated, and the biotinylated sample was subjected to the hydrolysis assay.

Observation of rotation

An observation chamber was constructed of a silanized bottom coverslip functionalized with Ni-NTA and an untreated top coverslip separated by two greased strips of Parafilm cover sheet (14).

Gold beads 40 nm in diameter were coated with polyethylene glycol (PEG) and functionalized with streptavidin as described elsewhere (26), with the following modifications: 62 μ M streptavidin (Pierce, Thermo Scientific, Rockford, IL) in buffer C (10 mM Mops-KOH, pH 7.0, 50 mM KCl) was thiolated by adding 0.5 mM dithiobis(succinimidyl propionate) in dimethyl sulfoxide and 10 mM of BondBreaker TCEP solution (Pierce) and letting the reaction proceed for 1 h at room temperature. PEG was also thiolated by mixing 20 mM NHS-dPEG24mer (Quanta BioDesign, Powell, OH) in dimethyl sulfoxide and 1 mM 2-aminoethanethiol in buffer C for 24 h at room temperature. Finally, gold beads (EM.GC40, BBI International, Cardiff, UK; a suspension at 9×10^{10} particles mL⁻¹) were modified by adding 625 nM thiolated streptavidin and 10 μ M thiolated PEG and letting the reaction proceed at room temperature for 2 h.

Biotinylated F₁ (0.5–1.5 nM) in buffer B was infused into the observation chamber, followed by bovine serum albumin (BSA) for surface blocking, functionalized gold beads, and finally buffer B with the addition of 2 mM MgATP and an ATP regenerating system (0.2 mg mL⁻¹ creatine kinase (rabbit muscle, Roche Diagnostics) and 2.5 mM creatine phosphate (Roche Diagnostics)); details of the infusion procedure can be found in Furuike et al. (26). Rotation of gold beads was observed by laser dark-field microscopy (26) on an inverted microscope (IX70, Olympus, Tokyo, Japan) with a stable mechanical stage (KS-O, ChuukoushaSeisakujo, Tokyo, Japan).

Images were captured with a high-speed CMOS camera (FASTCAM-DJV, Photron, Tokyo, Japan) at 125–8000 frames s⁻¹ as an 8-bit AVI file.

Rotation of polystyrene beads was observed in an observation chamber as described above. Streptavidin-coated beads of diameter 0.29 μ m (Seradyn, Indianapolis, IN) were washed and adjusted to a final concentration of 0.1% (w/v) in 5 mg mL⁻¹ BSA in buffer B. We infused into the observation chamber 0.5–2 nM F₁ in buffer B, BSA, streptavidin-coated beads, and buffer B containing 2 mM MgATP and the ATP regeneration system above, as described in detail in Hossain et al. (14). Polystyrene beads were observed by bright-field microscopy, and images were captured with a CCD camera (Lynx IPX-VGA210L, Imperx, Boca Raton, FL) at 500 frames s⁻¹ as an 8-bit AVI file. A duplex of beads was always selected for analysis.

All microscopic observations were made at 23°C. Centroid of the bead images was calculated as described previously (23). Rotating beads were counted as in Hossain et al. (27).

The torque, N , that the motor produced was estimated from the rotary speed, ω (in rad s⁻¹), of a 0.29- μ m bead duplex as (10,28)

$$N = \omega \xi, \quad (1)$$

where ξ is the frictional drag coefficient given, for the case of a duplex of spherical beads, by

$$\xi = 2 \times 8\pi\eta a^3 + 6\pi\eta a x_1^2 + 6\pi\eta a x_2^2, \quad (2)$$

where a is the bead radius, x_1 and x_2 the radii of the rotation of the inner and outer beads, and η is the viscosity of the medium (0.93×10^{-3} N·s·m⁻² at 23°C). We selected those duplexes with $x_2 > 0.2$ μ m; x_1 was taken as 0. The drag in Eq. 2 is likely an underestimate (10,29).

RESULTS

β - γ fusion and γ N-terminal truncations

We used as the wild-type an α (C193S)₃ β (His₁₀ at N-terminus)₃ γ (S107C, I210C) subcomplex of TF₁ (23). This subcomplex has only two cysteines at the protruding portion of the γ subunit for labeling with an external probe, and histidine tags at the bottom (N-terminus) of the β -subunits for attachment of the protein to a glass surface. In our previous γ truncation studies (11,12,14), purified mutant subcomplex tended to be unstable, particularly with large deletions. Hoping to mitigate this problem, we first fused γ and β : the gene for γ is immediately followed by a β gene on the expression plasmid, and thus, we simply inserted a sequence for the linker peptide (Fig. 1 D) and, in place of the β histidine tags removed for the linking, added six histidines to the N-terminus of α (Table S1, amino-acid sequences). We call the resultant construct β - γ Δ N0. The insertion on the gene level implies that all three β -subunits in a subcomplex carry a γ subunit. We included a thrombin site in the linker to cut it when desired. Starting with β - γ Δ N0, we truncated 8, 14, 29, 40, and 50 amino-acid residues from the N-terminus of γ to obtain β - γ Δ N8 to β - γ Δ N50. The linker was included in all these truncation mutants.

All mutants were expressed in *E. coli* to a level similar to that of the wild-type. Purified mutant subcomplexes showed two bands on SDS-PAGE, β - γ at progressively lower positions for larger truncations and α at a constant level, as

expected (Fig. 2). Treatment with thrombin produced β and truncated γ at the expense of β - γ , but some β - γ remained, and this persisted even after prolonged (18 h) treatment. Column purification of the subcomplex after thrombin treatment removed most of γ (and thrombin), but β - γ remained in the subcomplex in addition to α and β . The likely, though unproven, interpretation is that, of the three γ subunits in the untreated subcomplex, one was inserted into the $\alpha_3\beta_3$ cylinder and was resistant to thrombin.

Unloaded rotation probed with a 40-nm gold bead

We observed the rotation in the wild-type and mutants by attaching the stator part to a glass surface through the histidine tags at the α or β N-terminus and attaching a 40-nm gold bead at the top of the γ -subunit as a probe. The hydrodynamic friction on the 40-nm bead is practically negligible, warranting the observation of unloaded rotation (23) provided the bead is unobstructed and free to rotate in water. Rotation was observed at the saturating ATP concentration of 2 mM by laser dark-field microscopy (26) at 125–8000 frames s^{-1} . All mutants rotated counterclockwise for many continuous revolutions at a speed that decreased with the degree of truncation (Figs. 3 A and 4 A). The time-averaged speed of β - $\gamma\Delta N0$ was nearly as high as the wild-type speed, indicating that the covalent linkage between γ and β does not greatly impede rotation. This is not entirely unexpected, because a peptide chain contains many single bonds. Thrombin treatment did not affect the rotation speed in all mutants (Fig. 4).

Stepwise truncation resulted in corresponding decrease in the average speed until β - $\gamma\Delta N29$, beyond which the speed did not change appreciably. The lowest speed of ~ 50 revolutions s^{-1} amounts to a quarter of the wild-type speed and is 50 times higher than the axle-less mutant in Fig. 1 B. The constant nature beyond β - $\gamma\Delta N29$ is consistent with the structure in Fig. 1 A, where the upper portion of the N-terminal helix does not interact with the stator cylinder.

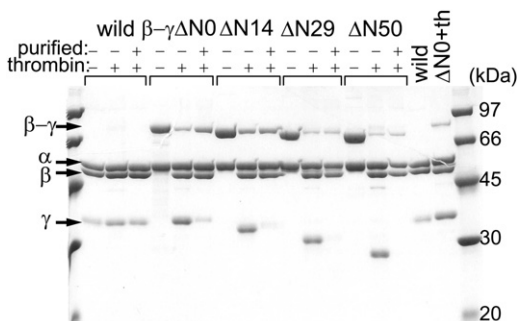


FIGURE 2 Confirmation of truncations using SDS-PAGE. Samples were run in a 12.5% gel containing 0.1% SDS, and then stained with Coomassie Brilliant Blue R-250. The three lanes for each construct are: --, purified subcomplex before thrombin treatment; - +, after thrombin treatment for 10 min (reaction mixture); + +, after further purification by size-exclusion chromatography.

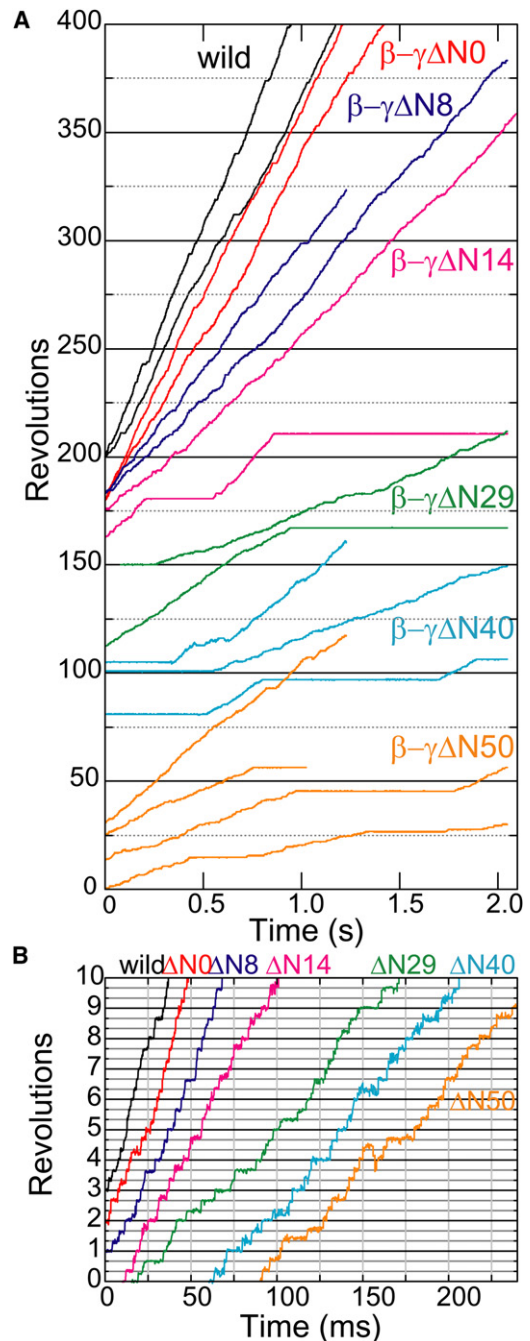


FIGURE 3 Rotation of 40-nm gold beads at 2 mM MgATP. (A) Representative overall time courses. (B) Magnified portions showing apparent 120° stepping recorded at 8000 frames s^{-1} . Most populated angles for each record (judged on the entire time course) are placed on the horizontal lines separated by 120° . The two successive backward 120° steps at ~ 160 s in β - $\gamma\Delta N50$ are exceptional clean back steps in all records analyzed for all mutants.

It also implies that the absence of the upper helix does not affect the rotor structure appreciably.

Magnified time courses in Fig. 3 B show that all mutants made short dwells every 120° , as did the wild-type (not well resolved in the chosen magnification). The dwells were

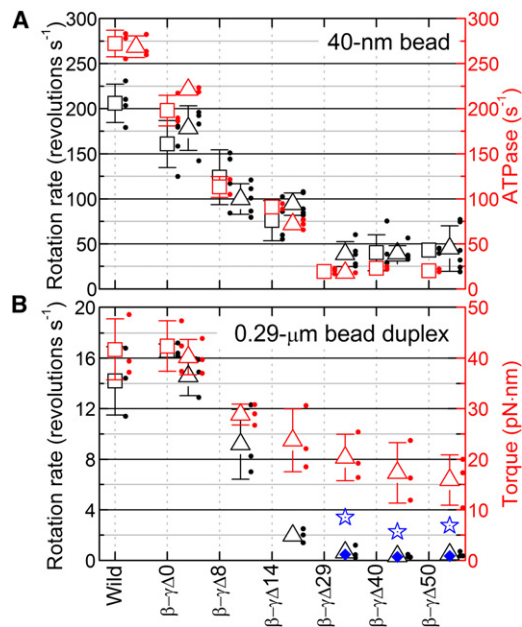


FIGURE 4 Summary of rotation and ATP hydrolysis properties of the N-terminal truncation mutants at 2 mM ATP. Average values for mutants without thrombin treatment are represented by squares on the vertical dotted lines, and those for mutants after thrombin treatment by triangles to the right of the dotted lines; error bars indicate \pm SD and are shown when their size exceeds the symbol size; dots show individual measurements. All data shown here were obtained within three days of preparation (samples were kept at room temperature). (A) Unloaded rotation rate probed with 40-nm gold beads (black) and bulk ATP hydrolysis rate (red). Time-averaged rotation rates were calculated over >100 consecutive revolutions for the wild-type to β - $\gamma\Delta N14$ and >20 revolutions for β - $\gamma\Delta N29$ to β - $\gamma\Delta N50$. Those beads that rotated relatively fast, with a nearly circular rotation trace with a central hole (large rotation radius), were analyzed. (B) Time-averaged rotation rates of the relatively fast bead duplexes estimated over 50 consecutive revolutions (black), and torque estimated from rotational steps of 0.29- μ m bead duplexes (red; see Fig. 6). Blue diamonds show the average of torque values estimated from the time-averaged rotation speeds (black dots), and blue stars the torque estimated from the time-averaged speed in the fastest portions (red in Fig. 5, A and B).

longer for shorter mutants, which is the major reason for the lower average speed. In the wild-type, the dwells observed at the saturating ATP of 2 mM are 80° past ATP-waiting angles, where ATP hydrolysis and phosphate release take place (23,30,31). Dwell positions in the mutants are unknown, but they are likely at $\sim 80^\circ$ as in the wild-type, because only dwells at 120° intervals were discerned in both the wild-type and mutants. Presumably, longer dwells in the mutants reflect inefficient coupling between chemical reactions in the catalytic sites and the γ rotation that is supposed to coordinate catalysis. More irregular rotations in the short mutants (Fig. 3 B) may reflect fluctuations of the half-sliced axle in the stator orifice. We also noticed that short mutants tended to fall in pauses for ~ 1 s (Fig. 3 A), at one of the dwelling angles. In the shortest mutants (β - $\gamma\Delta N29$ to β - $\gamma\Delta N50$), continuous rotation for 50 revolutions without a long pause was rare. The wild-type also falls

in long pauses at 80° , due to MgADP inhibition, but these pauses are longer on average and less frequent (32). The shortest mutants may be more prone to MgADP inhibition.

Finding rotating beads became difficult for shorter mutants. For the wild-type and β - $\gamma\Delta N0$, more than one bead rotated in most fields of view ($16 \times 16 \mu\text{m}^2$), but ~ 10 fields had to be scanned to find an easily identifiable rotating bead for the shortest three mutants. A quantitative estimate of the number of rotating 40-nm beads was difficult, because rotation with a small radius could not be detected reliably.

ATP hydrolysis activity

To compare with the unloaded rotation speeds, we measured the rate of ATP hydrolysis at 2 mM ATP in bulk samples. In this work, we did not remove the tightly bound nucleotide completely, and thus, part of the enzyme was under MgADP inhibition. We therefore measured the hydrolysis activity in the presence of LDAO, which reactivates F_1 from MgADP inhibition (33). The wild-type activity was 270 s^{-1} (Fig. 4 A), similar to or slightly less than the initial activity of nucleotide-depleted wild-type in the absence of LDAO (12,14). Thrombin treatment did not affect the wild-type activity as expected.

The hydrolysis activities of the mutants followed a trend basically similar to that of the unloaded rotation speed (Fig. 4 A). Linking alone (β - $\gamma\Delta N0$) reduced the activity slightly to 200 s^{-1} , and N-terminal truncation progressively reduced the activity further. Thrombin, where tested, did not affect the hydrolysis activity of the mutants (Fig. 4 A). The activities of the shortest three mutants (β - $\gamma\Delta N29$ to β - $\gamma\Delta N50$) were all 19 – 20 s^{-1} . These values are $\sim 7\%$ of the wild-type activity and much less than the expectation from the unloaded rotation speeds, probably due to the presence of destabilized subcomplex, but are still much higher than the rate of hydrolysis by the γ -less mutant ($\alpha_3\beta_3$ ring) of $\sim 5 \text{ s}^{-1}$ (12). The wild-type activity was also low compared to its unloaded rotation speed, as in previous studies (12,23,27), for a reason yet to be clarified.

Rotation of 0.29- μ m bead duplexes

All mutants were able to rotate a duplex of 0.29- μ m beads at 2 mM ATP, indicating significant torque generation. All rotated in the counterclockwise direction. The number of rotating duplexes was examined in five separate observation chambers and in 10 random fields for each chamber. In the case of the wild-type infused at 2 nM, 56 rotating bead duplexes were found in 50 fields of view (each $18.9 \times 14.4 \mu\text{m}^2$). Under the same conditions (2 nM protein), 41 duplexes rotated with β - $\gamma\Delta N0$, 26 with β - $\gamma\Delta N8$, 16 with β - $\gamma\Delta N14$, 2 with β - $\gamma\Delta N29$, 1 with β - $\gamma\Delta N40$, and 1 with β - $\gamma\Delta N50$. Rotation could be observed for at least 2 h after chamber preparation.

Rotation time courses observed at 500 frames s⁻¹ are shown in Fig. 5 A. Rotation of the wild-type and β - γ Δ N0 (with or without thrombin treatment) was too fast on the chosen scale: both rotated at \sim 16 revolutions s⁻¹ smoothly and continuously for >100 revolutions. This rotation speed is much lower than that of a 40-nm gold bead, limited by viscous friction against the 0.29- μ m bead duplex. N-terminal truncations resulted in progressively lower time-averaged speeds (Figs. 4 B and 5 A), largely due to longer and more frequent pauses (Fig. 5). Again, these speeds are much lower than corresponding rotations of the 40-nm beads, but the major cause is the longer pauses and not the hydrodynamic friction. Apparently, the fastest portion of rotation in β - γ Δ N29, β - γ Δ N40, and β - γ Δ N50 (Fig. 5, A and B, red) still contained many relatively short

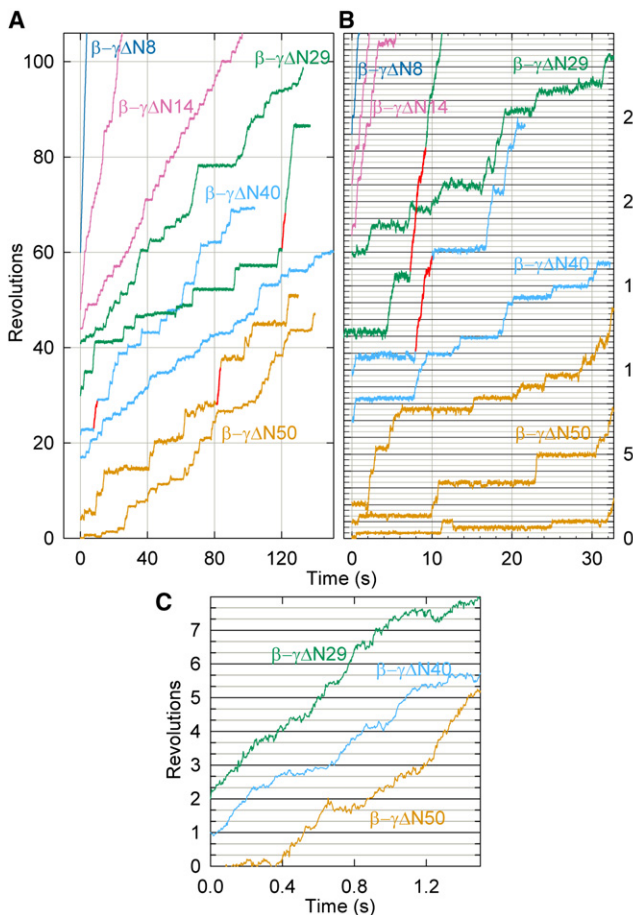


FIGURE 5 Rotation of 0.29- μ m bead duplexes at 2 mM MgATP. The wild-type and β - γ Δ N0 (with or without thrombin) both showed fast, continuous rotation at \sim 16 revolutions s⁻¹ and are not shown. (A) Relatively fast revolutions selected for each mutant. The three red portions in the time courses for β - γ Δ N29, β - γ Δ N40, and β - γ Δ N50 show the fastest six revolutions observed in these mutants (magnified in C). (B) Magnified records showing pauses of variable lengths. Red portions are as in A. Bottom curve shows an exceptional case of clear reversal over one 120° step in a sluggish phase. (C) Expanded views of the red portions in A, showing many short pauses.

pauses, as seen in the magnified records (Fig. 5 C). Our previous studies have indicated that the wild-type also shows a tendency to stumble at angles of \sim 80° past ATP-waiting angles in a load-dependent fashion: with a high load such as a duplex of 0.95- μ m beads, we often observed a momentary pause at these angles, but pauses were less conspicuous with smaller beads (28). Load dependence was also observed in the previous truncation mutants: γ Δ N0C25 to γ Δ N0C36, for example, could rotate a duplex of 0.29- μ m beads but not a duplex of 0.49- μ m beads (14), whereas γ Δ N0C21 could rotate a 0.49- μ m duplex (11). Presumably, the torque of the motor momentarily vanishes at the pausing angles, and larger beads somehow impede the escape from the pauses. Mutants are more sensitive, particularly those in which the rotor-stator interactions are largely impaired.

Torque of the mutants

The basically unidirectional rotation of the mutants implies torque generation, and the torque must be sizable to drive the duplex of 0.29- μ m beads. Because rotation of the mutants involved many pauses, we analyzed the instantaneous rotary speed in the middle of the 120° steps for torque estimation, assuming that the speed during stepping was limited by viscous friction against the bead duplex. We averaged 30 consecutive steps to obtain the thick cyan curves in Fig. 6, and calculated the torque as the slope of the cyan curve between 30° and 90° times the frictional drag coefficient of the bead duplex (Eqs. 1 and 2 in Methods). The apparent sluggishness outside the 30–90° region likely resulted from the simple averaging of noisy and ill-synchronized steps.

The torque values thus estimated are summarized in Fig. 4 B. Rotor-stator linkage alone (β - γ Δ N0) did not affect the torque, but N-terminal truncations considerably reduced the torque. Yet the shortest mutants, β - γ Δ N29 to β - γ Δ N50, produced about half the wild-type torque. Because the step records for these mutants were highly noisy (Fig. 6), we made additional torque estimates to set lower bounds. One is to apply Eq. 1 to the time-averaged rotation speed for consecutive 50 revolutions (Fig. 4 B, black dots). The average speed is unambiguous, confirming the generation of finite torque by these mutants, but it is clear that the obtained torque values (Fig. 4 B, blue diamonds) are underestimated greatly, because none of the pauses are taken into account. The fastest six revolutions (Fig. 5, red) contained relatively short pauses, and thus, their average speeds gave higher torque values (Fig. 4 B, blue stars). Portions nearly as fast could be found in many places in the records.

DISCUSSION

Without the entire N-terminal α -helix of the γ rotor, TF₁ rotates in the correct direction at an unloaded speed a quarter

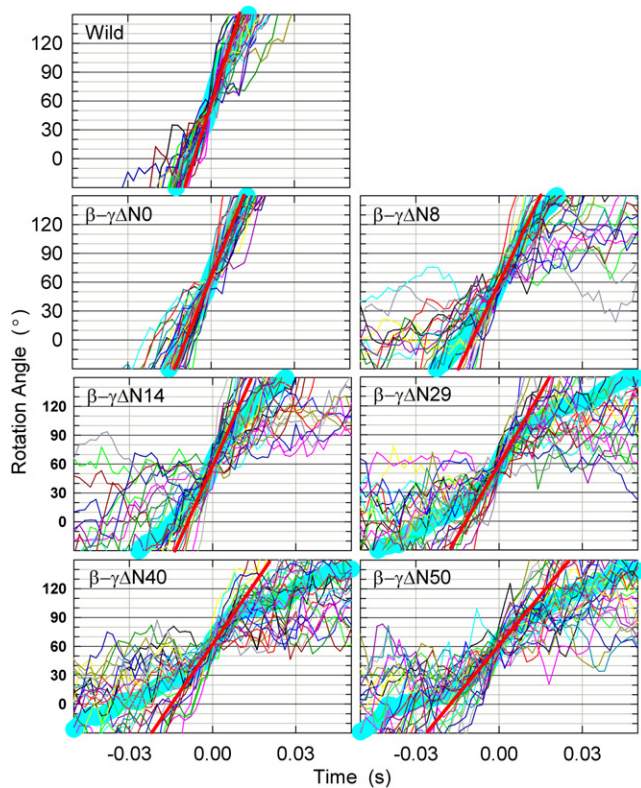


FIGURE 6 Step records of 0.29- μm bead duplexes for torque estimation. Thin colored curves show 30 consecutive 120° steps; thick cyan curves represent their average. Individual step records were shifted vertically by a multiple of 120° to obtain overlap. Time zero for each step record was assigned by eye to the data point closest to 60°. Straight red lines indicate linear fit to the cyan curve between 30° and 90°. The slope of the red line, ω , gives the torque, N (Eq. 1).

of the wild-type speed and generates half the wild-type torque. Among the three heavily truncated mutants shown in Fig. 1, the N-terminal truncation in this work (Fig. 1 A) and C-terminal truncation (Fig. 1 C) could rotate a duplex of 0.29- μm beads, generating around half the wild-type torque, whereas the axle-less mutant (Fig. 1 B) could rotate only a 40-nm bead very slowly (~ 1 revolution s^{-1}). Because the orifice interactions were mostly preserved in the C-terminal truncation, whereas further truncation (removal of the red residues in Fig. 1 C: $\gamma\Delta\text{N}0\text{C}40$) failed to rotate the bead duplex, it appears that either full interactions at the orifice (Fig. 1 C) or approximately half of the orifice interactions supplemented with the sleeve interactions (Fig. 1 A) suffice to generate a sizable torque. The F_1 motor appears robust in that none of the rotor parts are critically important, suggesting the possibility that the $\alpha_3\beta_3$ stator might be able to rotate an object that does not bear resemblance to the γ subunit.

One possibly crucial rotor component still remains, however. The collar of the rotor that touches the conical entrance of the stator orifice, except the part on the N-terminal helix, is common to all three mutants in Fig. 1.

This non-N-terminal part of the collar, including a short helix 73–90 (in $\text{MF}_1\text{-}\gamma$ (8)), may thus be essential for rotation. The non-N-terminal collar interacts mainly with the highly conserved and highly acidic DELSEED motif ($\beta\text{-Asp-394}$ to $\beta\text{-Asp-400}$ in MF_1), the dark green atoms at the top of β_{TP} in Fig. 1 A and those atoms in β_{DP} (not shown) that oppose the brown atoms in the right ellipse in Fig. 1 B. The collar was preserved in the axle-less mutant (Fig. 1 B), and if the remaining rotor head had somehow been pulled inward to let the collar firmly interact with the stator orifice, the axle-less rotor head might have been able to generate a sizable torque. Because all the negatively charged residues of the DELSEED motif could be replaced with alanine without affecting the torque (34), it is not highly likely that the rotor collar is an essential component. Direct proof, though, is awaited.

SUPPORTING MATERIAL

A table and references are available at [http://www.biophysj.org/biophysj/supplemental/S0006-3495\(11\)00578-9](http://www.biophysj.org/biophysj/supplemental/S0006-3495(11)00578-9).

We thank R. Shimo-Kon and other members of the Kinosita lab for technical advice and discussion, and S. Takahashi, K. Sakamaki, and M. Fukatsu for encouragement and laboratory management.

This work was supported by Grants-in-Aid for Specially Promoted Research from the Ministry of Education, Culture, Sports, Science, and Technology of Japan. M.D.H. was supported by a postdoctoral fellowship from the Japan Society for the Promotion of Science.

REFERENCES

- Boyer, P. D. 1997. The ATP synthase—a splendid molecular machine. *Annu. Rev. Biochem.* 66:717–749.
- Noji, H., R. Yasuda, ..., K. Kinosita, Jr. 1997. Direct observation of the rotation of $F_1\text{-ATPase}$. *Nature.* 386:299–302.
- Kinosita, Jr., K., R. Yasuda, ..., K. Adachi. 2000. A rotary molecular motor that can work at near 100% efficiency. *Philos. Trans. R. Soc. Lond. B Biol. Sci.* 355:473–489.
- Yoshida, M., E. Muneyuki, and T. Hisabori. 2001. ATP synthase—a marvellous rotary engine of the cell. *Nat. Rev. Mol. Cell Biol.* 2:669–677.
- Senior, A. E., S. Nadanaciva, and J. Weber. 2002. The molecular mechanism of ATP synthesis by $F_1F_0\text{-ATP synthase}$. *Biochim. Biophys. Acta.* 1553:188–211.
- Kinosita, Jr., K., K. Adachi, and H. Itoh. 2004. Rotation of $F_1\text{-ATPase}$: how an ATP-driven molecular machine may work. *Annu. Rev. Biophys. Biomol. Struct.* 33:245–268.
- Junge, W., H. Sielaff, and S. Engelbrecht. 2009. Torque generation and elastic power transmission in the rotary $F_0F_1\text{-ATPase}$. *Nature.* 459:364–370.
- Abrahams, J. P., A. G. W. Leslie, ..., J. E. Walker. 1994. Structure at 2.8 Å resolution of $F_1\text{-ATPase}$ from bovine heart mitochondria. *Nature.* 370:621–628.
- Gibbons, C., M. G. Montgomery, ..., J. E. Walker. 2000. The structure of the central stalk in bovine $F_1\text{-ATPase}$ at 2.4 Å resolution. *Nat. Struct. Biol.* 7:1055–1061.
- Yasuda, R., H. Noji, ..., M. Yoshida. 1998. $F_1\text{-ATPase}$ is a highly efficient molecular motor that rotates with discrete 120° steps. *Cell.* 93:1117–1124.

11. Hossain, M. D., S. Furuike, ..., K. Kinosita, Jr. 2006. The rotor tip inside a bearing of a thermophilic F₁-ATPase is dispensable for torque generation. *Biophys. J.* 90:4195–4203.
12. Furuike, S., M. D. Hossain, ..., K. Kinosita, Jr. 2008. Axle-less F₁-ATPase rotates in the correct direction. *Science*. 319:955–958.
13. Shirakihara, Y., A. G. W. Leslie, ..., M. Yoshida. 1997. The crystal structure of the nucleotide-free $\alpha_3\beta_3$ subcomplex of F₁-ATPase from the thermophilic *Bacillus* PS3 is a symmetric trimer. *Structure*. 5:825–836.
14. Hossain, M. D., S. Furuike, ..., K. Kinosita, Jr. 2008. Neither helix in the coiled coil region of the axle of F₁-ATPase plays a significant role in torque production. *Biophys. J.* 95:4837–4844.
15. Kanazawa, H., H. Hama, ..., M. Futai. 1985. Deletion of seven amino acid residues from the γ subunit of *Escherichia coli* H⁺-ATPase causes total loss of F₁ assembly on membranes. *Arch. Biochem. Biophys.* 241:364–370.
16. Shin, K., R. K. Nakamoto, ..., M. Futai. 1992. F₀F₁-ATPase γ subunit mutations perturb the coupling between catalysis and transport. *J. Biol. Chem.* 267:20835–20839.
17. Omote, H., N. Sambonmatsu, ..., M. Futai. 1999. The γ -subunit rotation and torque generation in F₁-ATPase from wild-type or uncoupled mutant *Escherichia coli*. *Proc. Natl. Acad. Sci. USA*. 96:7780–7784.
18. Feniouk, B. A., A. Rebecchi, ..., B. A. Melandri. 2007. Met23Lys mutation in subunit gamma of F₀F₁-ATP synthase from *Rhodobacter capsulatus* impairs the activation of ATP hydrolysis by protonmotive force. *Biochim. Biophys. Acta*. 1767:1319–1330.
19. Lowry, D. S., and W. D. Frasch. 2005. Interactions between β D372 and γ subunit N-terminus residues γ K9 and γ S12 are important to catalytic activity catalyzed by *Escherichia coli* F₁F₀-ATP synthase. *Biochemistry*. 44:7275–7281.
20. Ni, Z.-L., H. Dong, and J. M. Wei. 2005. N-terminal deletion of the γ subunit affects the stabilization and activity of chloroplast ATP synthase. *FEBS J.* 272:1379–1385.
21. Dian, E. A., P. Papatheodorou, ..., C. Motz. 2008. Role of γ -subunit N- and C-termini in assembly of the mitochondrial ATP synthase in yeast. *J. Mol. Biol.* 377:1314–1323.
22. Gumbiowski, K., D. Cherepanov, ..., S. Engelbrecht. 2001. F-ATPase: forced full rotation of the rotor despite covalent cross-link with the stator. *J. Biol. Chem.* 276:42287–42292.
23. Yasuda, R., H. Noji, ..., H. Itoh. 2001. Resolution of distinct rotational substeps by submillisecond kinetic analysis of F₁-ATPase. *Nature*. 410:898–904.
24. Matsui, T., and M. Yoshida. 1995. Expression of the wild-type and the Cys-/Trp-less $\alpha_3\beta_3\gamma$ complex of thermophilic F₁-ATPase in *Escherichia coli*. *Biochim. Biophys. Acta*. 1231:139–146.
25. Adachi, K., H. Noji, and K. Kinosita, Jr. 2003. Single-molecule imaging of rotation of F₁-ATPase. *Methods Enzymol.* 361:211–227.
26. Furuike, S., K. Adachi, ..., K. Kinosita, Jr. 2008. Temperature dependence of the rotation and hydrolysis activities of F₁-ATPase. *Biophys. J.* 95:761–770.
27. Hossain, M. D., S. Furuike, ..., K. Kinosita, Jr. 2010. Stimulation of F₁-ATPase activity by sodium dodecyl sulfate. *Biochim. Biophys. Acta*. 1797:435–442.
28. Sakaki, N., R. Shimo-Kon, ..., K. Kinosita, Jr. 2005. One rotary mechanism for F₁-ATPase over ATP concentrations from millimolar down to nanomolar. *Biophys. J.* 88:2047–2056.
29. Pänke, O., D. A. Cherepanov, ..., W. Junge. 2001. Viscoelastic dynamics of actin filaments coupled to rotary F-ATPase: angular torque profile of the enzyme. *Biophys. J.* 81:1220–1233.
30. Adachi, K., K. Oiwa, ..., K. Kinosita, Jr. 2007. Coupling of rotation and catalysis in F₁-ATPase revealed by single-molecule imaging and manipulation. *Cell*. 130:309–321.
31. Shimabukuro, K., R. Yasuda, ..., M. Yoshida. 2003. Catalysis and rotation of F₁ motor: cleavage of ATP at the catalytic site occurs in 1 ms before 40° substep rotation. *Proc. Natl. Acad. Sci. USA*. 100:14731–14736.
32. Hirono-Hara, Y., H. Noji, ..., M. Yoshida. 2001. Pause and rotation of F₁-ATPase during catalysis. *Proc. Natl. Acad. Sci. USA*. 98:13649–13654.
33. Jault, J.-M., C. Dou, ..., W. S. Allison. 1996. The $\alpha_3\beta_3\gamma$ subcomplex of the F₁-ATPase from the thermophilic bacillus PS3 with the β T165S substitution does not entrap inhibitory MgADP in a catalytic site during turnover. *J. Biol. Chem.* 271:28818–28824.
34. Hara, K. Y., H. Noji, ..., M. Yoshida. 2000. The role of the DELSEED motif of the β subunit in rotation of F₁-ATPase. *J. Biol. Chem.* 275:14260–14263.
35. Wang, H., and G. Oster. 1998. Energy transduction in the F₁ motor of ATP synthase. *Nature*. 396:279–282.